Shot noise in transport through quantum dots: ballistic versus diffractive scattering

Stefan Rotter,[a,b,*] Florian Aigner,[b] and Joachim Burgdörfer[b]

[a]Department of Applied Physics, Yale University, New Haven, CT 06520, USA
[b]Institute for Theoretical Physics, Vienna University of Technology, A-1040 Vienna, Austria

ABSTRACT

We investigate the shot noise in phase-coherent transport through quantum cavities by a two dimensional ab-initio simulation of the scattering problem. In particular, we study the influence of quantum scattering mechanisms on the transport statistics by tuning the strength of a disorder potential and the openings of the dot. For small cavity openings we find the shot noise for disordered samples to be of almost equal magnitude as for clean samples where transport is ballistic. We explain this finding by diffractive scattering at the cavity openings which act as strong noise sources. For ballistic cavities we demonstrate the emergence of "noiseless scattering states", irrespective of sharp-edged entrance and exit lead mouths. Our numerical results for the onset thresholds of these "classical" states are in very good agreement with analytical estimates.

Keywords: Shot noise, full counting statistics, quantum dots, disorder, mesoscopic transport, quantum chaos.

1. INTRODUCTION

Now almost a century ago Walter Schottky investigated the shot noise in vacuum tubes and explained this phenomenon by the granularity of the electron charge.[1] Recently this topic has resurfaced in the field of *mesoscopic physics*,[2,3] as it was shown that the phase-coherent current through low temperature conductors shows very distinct shot noise characteristics. Ballistic quantum transport experiments[4,5] as well as theoretical investigations[6–15] have demonstrated that the time-dependent current shot noise contains very useful information about the system properties of a conductor. This information has, e.g., been used to explore the crossover from a deterministic (classical) particle picture of electron motion to a probabilistic (quantum) description, where electrons behave as matter waves.[4,6–15] Contrary to the classical vacuum tube where the noise is due to the random emission of charges, it is the quantum uncertainty inherent in phase-coherent transport which gives rise to current shot noise in mesoscopic systems. Due to the correlations between electrons in the Fermi sea the mesoscopic shot noise S is suppressed relative to the Poissonian value of uncorrelated electrons S_P.[6] This suppression is customarily expressed in terms of the Fano factor $F = S/S_P$.

Most investigations to date have focused on mesoscopic quantum dots whose dynamics is fully chaotic or fully stochastic. In this limit random matrix theory (RMT)[16] predicts a universal value for the Fano factor, $F = 1/4$. The applicability of this RMT result requires, however, dwell times in the open cavity, τ_D, which are sufficiently long compared to the characteristic quantum scattering time τ_Q in the cavity potential. The latter estimates the time for the initially localized quantum wavepackets to be scattered into random direction and thus to be spread all over the width d of the cavity (typically $d \approx \sqrt{A}$ with A area of the dot). The limit $\tau_Q/\tau_D \ll 1$ corresponds to the quantum (or RMT) regime and $\tau_Q/\tau_D \gg 1$ corresponds to the classical limit for which $F = 0$ is expected. For cavities where τ_Q is determined by stochastic quantum scattering at a disorder potential, a simple conjecture for the quantum-to-classical crossover of F was put forward,[4,11]

$$F \approx 1/4 \, (1 + \tau_Q/\tau_D)^{-1} \, . \tag{1}$$

We note at this point that a similar prediction was presented for the case that the spreading of the wavepacket in the cavity is due to classical chaotic dynamics.[7] In the case we study here, the noise source is however given by a short-range disorder potential and Eq. (1) should be applicable. The term "short-range" refers to the

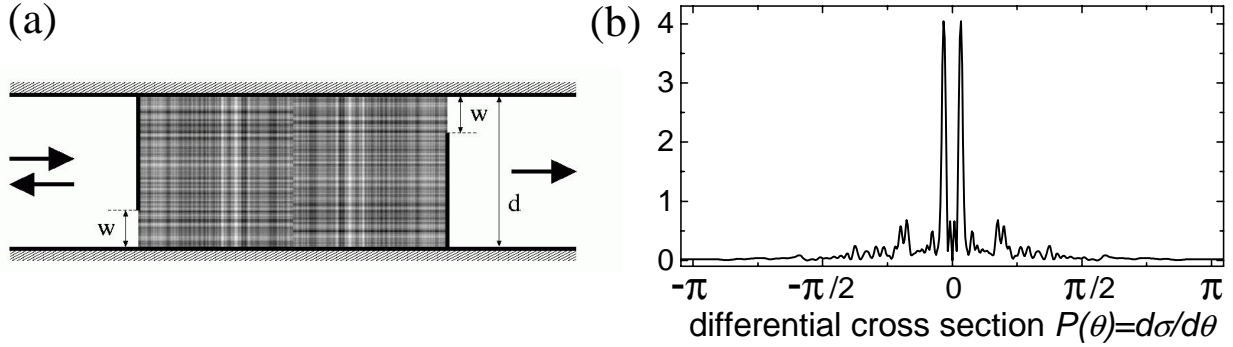* Electronic address: stefan.rotter@yale.edu

Figure 1. (a) Rectangular quantum billiard with tunable shutters and disorder potential (gray shaded area). Electrons are injected from the left into the cavity region of size $A = 2d^2$, width $2d$ and height d. Tuning the opening of the shutters w and the strength of the disorder potential V_0, the crossover from quantum-to-classical and disordered-to-ballistic scattering can be investigated, respectively. (b) Normalized differential scattering probability $P(\theta) \sim d\sigma/d\theta$ as calculated in first Born approximation for the disorder potential in (a). Note the two prominent peaks at small angles, indicating a strong bias towards forward-scattering (similar to observations in the experiment[17]).

correlation length of the disorder, l_C, which must be smaller than the Fermi wavelength λ_F. The scattering of wavepackets at this potential is thus determined by stochastic quantum diffraction rather than by classical scattering mechanisms. The strength and shape of the disorder potential will control the amount of diffractive scattering that enters τ_Q. The shot noise and its crossover from the disordered (quantum) regime to the clean (classical) regime is eventually determined by the ratio τ_Q/τ_D in Eq. (1).

An obvious test of the above prediction would be to simulate phase-coherent scattering processes on a computer. However, conventional numerical techniques suffer from a slow convergence rate, especially for the case where many open modes participate in the transport process. To circumvent this difficulty an "open" dynamical kicked rotator model was recently successfully used to mimic chaotic as well as stochastic scattering in a 1D-system.[9,10,15,18]

2. NUMERICAL SIMULATION

The aim of the present paper is to investigate the above questions by numerically simulating the full two-dimensional quantum transport problem for the case of a disordered cavity. Our quantum calculation proceeds within the framework of the modular recursive Green's function method (MRGM)[19] which overcomes some of the limitations of conventional techniques and allows us to perform transport calculations for two-dimensional quantum dots with relatively small λ_F. By decreasing the disorder strength in our quantum cavity, we can explore the predicted suppression of shot noise to the limit of vanishing disorder amplitude where transport is ballistic. Note that in the ballistic limit of this crossover one might expect a complete suppression of shot noise ($F = 0$), corresponding to the limit $\tau_Q \to \infty$ in Eq. (1). We will demonstrate in the following that this noiseless classical limit is not realized in realistic scattering systems, as also other noise sources will contribute significantly.

Our scattering system consists of a rectangular cavity to which two leads of width d are attached via tunable shutters with an opening width w (see Fig. 1a). The cavity region of width d and length $2d$ contains a static on-site disorder potential V characterized by its mean value $\langle V \rangle = 0$, and the correlation function $\langle V(x)V(x+a) \rangle = \langle V^2 \rangle \exp(-a/l_C)$. As required for a short-range disorder potential, we choose the correlation length l_C to be a small fraction of the Fermi wavelength $l_C/\lambda_F \approx 0.12$. Setting the potential strength $V_0 = \sqrt{\langle V^2 \rangle}$ to be weak, $V_0/E_F \leq 0.1$, we avoid that the electrons show any kind of localization in the disorder. Separately varying the lead openings and the amplitude of the disorder potential allows us to tune the dwell time τ_D and the rate of stochastic scattering in the cavity independently of each other. Note that in the ballistic limit of vanishing disorder ($V_0 \to 0$) our cavity becomes a clean rectangular box featuring only regular (integrable) classical dynamics. We evaluate the transmission amplitudes t_{mn} for an electron injected from the left by projecting the Green's function at the Fermi energy $G(E_F)$ onto all modes $m, n \in [1, \ldots, N]$ in the in- and outgoing lead,
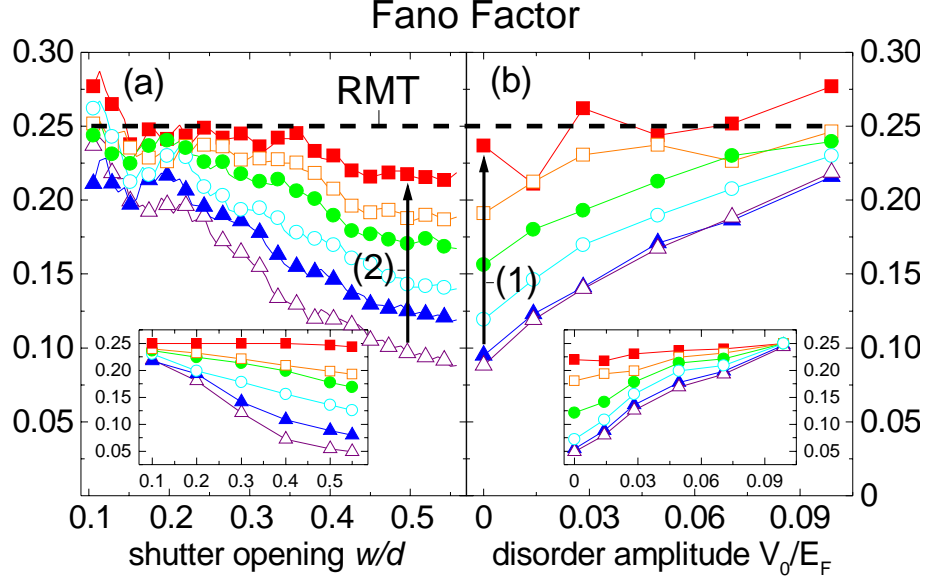
Figure 2. (a) Fano factor F for the cavity shown in Fig. 1a as a function of the shutter opening ratio w/d (both cavity openings always have the same size). Curves for different disorder amplitudes: $V_0/E_F = 0.1 (\blacksquare)$, $0.07 (\square)$, $0.05 (\bullet)$, $0.03 (\circ)$, $0.015 (\blacktriangle)$, $0 (\triangle)$. The universal "quantum" value $F = 1/4$ [as predicted by random matrix theory (RMT)] is well reproduced for small shutter openings (large large τ_D); large deviations towards the "classical value" $F = 0$ occur for large cavity openings (short τ_D). (b) Fano factor as a function of the disorder amplitude V_0. Curves for different shutter openings: $w/d = 0.1 (\blacksquare)$, $0.2 (\square)$, $0.3 (\bullet)$, $0.4 (\circ)$, $0.5 (\blacktriangle)$, $0.55 (\triangle)$. The black vertical arrows indicate two crossover trajectories (1) and (2) as discussed in the text. Insets of (a) and (b) depict the theoretical prediction (without fit parameters) based on a quasiclassical simulation and Eq. (3). Note the good agreement with the numerical data from the full quantum calculation.

respectively. The Fano factor F is then calculated[3] from the N-dimensional matrix of transmission amplitudes t,

$$F = \frac{\langle \text{Tr } t^\dagger t(1 - t^\dagger t)\rangle}{\langle \text{Tr } t^\dagger t\rangle} = \frac{\langle \sum_{n=1}^{N} T_n(1 - T_n)\rangle}{\langle \sum_{n=1}^{N} T_n\rangle}, \qquad (2)$$

with T_n being the eigenvalues of $t^\dagger t$. The brackets $\langle \ldots \rangle$ indicate that we average over 150 equidistant points in the wavenumber-range $k_F \in [40.1, 40.85] \times \pi/d$, where 40 transverse lead modes are open. We choose a nearest-neighbor spacing $\Delta x = \Delta y$ in the Cartesian discretization grid such that the Fermi wavelength is well resolved by a large number of grid points, $\lambda_F \approx 32\Delta x$. With these settings we have a total number of $\sim 8.5 \times 10^5$ grid points in the interior of the cavity.

3. SHOT NOISE RESULTS

The numerical results for the Fano factor F are displayed in Fig. 2 as a function of the shutter opening w/d (Fig. 2a) and the disorder amplitude V_0 (Fig. 2b). For small shutter openings $w/d \to 0$ (i.e. large dwell times) F approaches the universal value $1/4$ irrespective of the strength of the disorder potential V_0, while for wider openings (shorter dwell times) F falls off gradually. The steepness of this decrease is clearly dependent on V_0 and thus on the strength of disorder scattering. Most striking is the feature that for $V_0 \to 0$ but long dwell times the shot noise reaches the RMT value even though the dynamics is now entirely regular. In Fig. 2b this feature is reflected by the fact that the Fano factor F does not decay to zero even as $V_0 \to 0$ (compare also to similar results obtained from magnetotransport calculations[13]). This observation suggests that either the quantum scattering time τ_Q contains additional contributions other than from disorder scattering alone, or that Eq. (1) requires a modification to properly account for the shot noise in the ballistic limit. We argue that the key point here is the wavepacket diffraction at the cavity openings which has to be incorporated in the theoretical description of shot noise.[20, 21] Note that this feature is inherent in quantum transport and independent of the disorder potential in

the cavity. Disorder scattering certainly leads to wavepacket spreading but does not constitute the only or, in general, dominant source. As will be shown below, incorporating diffraction at the cavity openings necessitates modifications both to Eq. (1) and to an estimate for the quantum scattering time τ_Q.

To quantify the total amount of diffraction by all different scattering sources in the cavity we perform a quasi-classical Monte-Carlo transport simulation in which we follow an ensemble of classical trajectories subject to diffractive scattering at the shutter openings[20] and to a Poissonian scattering process in the disorder potential region.[22] Diffraction at the cavity openings has been studied in detail[20, 21] and can be described by a standard Fraunhofer diffraction analysis for electrons which enter or leave the cavity.[20] In our quasi-classical simulation we therefore choose the initial momentum distribution of the injected electron trajectories to follow the analytical Fraunhofer diffraction patterns. To assess the Poissonian scattering off the disorder we calculate the transport mean free path $(\tau_S \cdot v_F)$ and the differential scattering probability $(P(\theta) \sim d\sigma/d\theta)$ in first Born approximation. We find that the differential cross section is strongly peaked at small forward scattering angles (see Fig. 1b) rather than being uniformly distributed among all angular directions (as one would expect for s-wave scattering). Our quasi-classical simulation allows us to determine a modified quantum scattering time $\widetilde{\tau}_Q$ as the time it takes for the ensemble of trajectories to acquire a mean spread of the order of the cavity width d under the influence of both Fraunhofer diffraction and multiple disorder scattering events in the cavity. In other words, the time $\widetilde{\tau}_Q$ is extracted from our numerics by checking at which moment in time the mean spreading $\Delta r(t)$ satisfies the following relation: $\Delta r(\widetilde{\tau}_Q) = \langle (\vec{r} - \langle \vec{r} \rangle)^2 \rangle^{1/2} = d$. We find that the inclusion of Fraunhofer scattering leads to a drastic reduction of the quantum scattering time $\widetilde{\tau}_Q$. An important consequence of this modification is that the parameter $\widetilde{\tau}_Q$ is now of comparable magnitude or even smaller than the time τ_0 beyond which a universal decay behavior for $P(t)$ can be expected to set in. In this regime (where $\widetilde{\tau}_Q \lesssim \tau_0$) system-specific deviations of the dwell time distribution from a universal decay law are more pronounced than characteristic mean differences between ballistic and stochastic cavities. For our estimate of the Fano factor F we therefore take into account the exact dwell time distribution $P(t)$, resulting from the quasi-classical simulation for the particular system we study. These ingredients determine the Fano factor F as follows:[8]

$$F = 1/4 \left[1 - \int_0^{\widetilde{\tau}_Q} P(t)\, dt \right] = 1/4 \int_{\widetilde{\tau}_Q}^{\infty} P(t)\, dt. \tag{3}$$

Note that this expression is applicable to disordered, chaotic as well as regular systems and should therefore be valid irrespective of whether the origin of spreading is ballistic scattering at the boundary or diffractive scattering inside the cavity. To check the validity of this approach, we compare the estimates obtained from Eq. (3) with the results from the full quantum calculation. As shown in the insets of Fig. 2a,b, we find the quasi-classical results to be in very good agreement with the numerical values from the quantum solution of the transport problem.

4. BALLISTIC VERSUS STOCHASTIC TRANSPORT

As displayed in Fig. 2a,b the shot noise power is increased by both an increase in the disorder strength V_0 as well as by a decrease in the shutter openings w/d. To illustrate the similarity between the effects of varying V_0 and w/d, let us compare two "crossover trajectories" in the two-dimensional parameter space of V_0 and w/d. We choose both trajectories to start from the same parameter values of vanishing disorder strength, $V_0 = 0$, and an opening ratio $w/d = 0.5$. As expected, the Fano factor F at this point in the ballistic limit ($V_0 = 0$) is rather low, $F \approx 0.1$. Consider now the increase of F either by (1) decreasing the shutter opening (without adding any disorder) or by (2) increasing the disorder strength in the cavity (at a fixed value of the cavity opening). Both crossovers trajectories (1),(2) are indicated by black arrows in Figs. 2a,b and apparently give rise to a very similar evolution of the Fano factor F. We therefore conclude that characteristic differences between the crossovers (1) and (2) are hard to pin down in the shot noise power. At first glance this finding might seem surprising, especially in view of the fact that in the absence of disorder [as in crossover (1)] shot noise suppression was predicted to be mediated by so-called "noiseless scattering states".[8] However, in the presence of disorder [as in crossover (2)] these noiseless states should be entirely suppressed. Noiseless (or deterministic) transport channels are expected to appear as soon as classical transmission bands[20] in phase space can be resolved by the
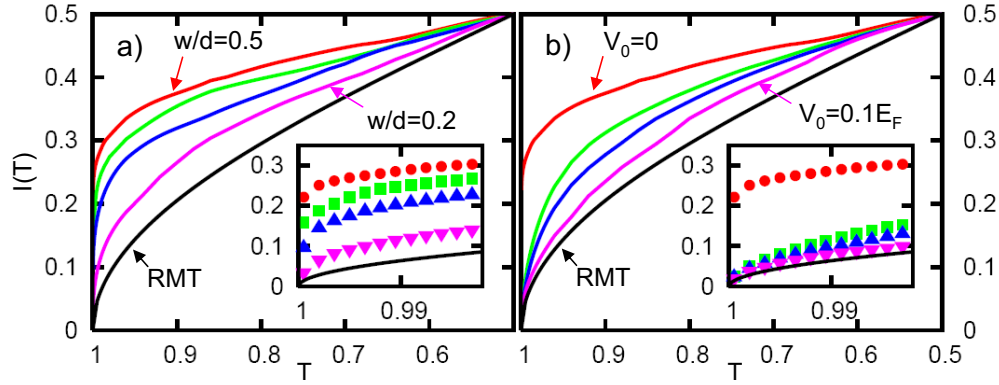
Figure 3. Integrated distribution function of transmission eigenvalues, $I(T)$, for the cavity shown in Fig. 1a. (a) Crossover from large to small shutter openings as indicated by arrow (1) in Fig. 2b (at zero disorder, $V_0 = 0$): I(T) for $w/d = 0.5, 0.4, 0.3$, and 0.2 (top to bottom). (b) Crossover from clean to disordered samples as indicated by arrow (2) in Fig. 2a (at half-opening, $w/d = 0.5$): I(T) for different disorder potentials $V_0 = 0, 0.03E_F, 0.05E_F$, and $0.1E_F$ (top to bottom). The pronounced difference between (a) and (b) near $T = 1$ is highlighted in the insets.

ballistic scattering process.[8, 10] The resulting separation of phase space in noiseless classical and noisy quantum channels is in sharp contrast to the case of cavities with bulk disorder where the formation of noiseless states is hindered by stochastic scattering and all transporting channels contribute to shot noise.[11, 15] As the crossovers (1) and (2) therefore can be expected to be governed by different scattering scenarios, we should be able to find signatures of these differences.

To uncover the presence and the decay of noiseless states in our numerical results we decide to investigate how the transmission eigenvalues T_n are statistically distributed for the two crossovers (1) and (2).[10, 11, 15] For classically chaotic systems with a large number of transporting channels ($N \gg 1$) and time reversal symmetry, random matrix theory (RMT) predicts that the distribution function of transmission eigenvalues, $P(T)$, follows a bimodal universal form,[16]

$$P_{RMT}(T) = \pi^{-1} [T(1-T)]^{-1/2}, \quad T \in [0,1] \quad \text{for which} \quad F = 1/4. \tag{4}$$

The appearance of "noiseless states" in ballistic scattering systems however entails a modification[8, 10] to this formula, especially around the classical transmission eigenvalues 0 or 1,

$$P^\alpha(T) = \alpha\, P_{RMT}(T) + (1-\alpha)\, [\delta(T) + \delta(1-T)]/2 \quad \text{for which} \quad F = \alpha/4. \tag{5}$$

The weight $(1 - \alpha)$ of the "noiseless states" in this "ballistic crossover" is determined by the degree with which the quantum scattering process can resolve finite-size transmission bands in the classical transport phase space. Ideally, the continuous crossover parameter α can take all values between the classical limit $\alpha = 0$ (for $\lambda_F/d \to 0$) and the quantum limit $\alpha = 1$ of low mode numbers, respectively.

In the presence of a uniform disorder with a correlation length smaller than the electron wavelength λ_F ("short-range bulk disorder") the formation of noiseless states is suppressed by stochastic scattering, leading to a different crossover form,[11]

$$P^\gamma(T) = P_{RMT}(T)\, \gamma \int\limits_{-1}^{1} du\, \frac{(1-u^2)|u|^{(2\gamma-1)}}{(1+u)^2 - 4Tu}\,, \tag{6}$$

resulting in Eq. (1) with $\gamma = \tau_Q/\tau_D$. This *stochastic* crossover, Eq. (6), interpolates between the same limiting cases P_{RMT} (for $\gamma \to 0$) and $P_{cl} = [\delta(T) + \delta(1 - T)]/2$ (for $\gamma \to \infty$, i.e. vanishing disorder) as the *ballistic* crossover in Eq. (5). Note that in the presence of both ballistic *and* stochastic scattering sources, Eqs. (5) and (6) should be appropriately combined to be predictive for our scattering system.[14] Equations (5) and (6), however, indicate qualitatively the different ways in which the transition between the limits P_{RMT} and P_{cl} are
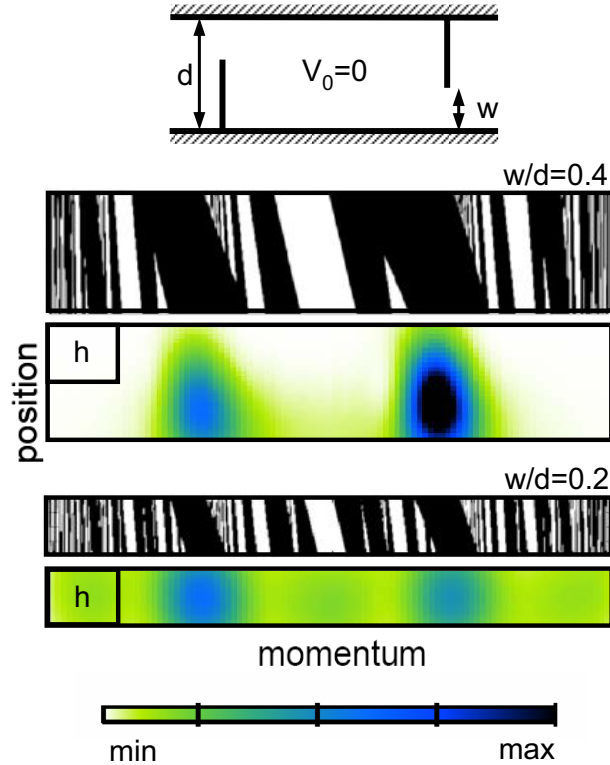
Figure 4. Quantum-to-classical correspondence in the cavity of Fig. 1a (no disorder, $V_0 = 0$): We compare the classical Poincaré surface of section as recorded at the left cavity opening (transmitted/reflected trajectories represented by black/white regions) with the cumulative Husimi distributions $H(x,p)$ of strongly transmitted scattering states, Eq. 7 (see color scale on bottom). The black frames plotted in the upper left corner of the Husimi distributions indicate the size of the Planck cell h. For the configuration with large shutter openings ($w/d = 0.4$, top two bars) the size of the Planck cell is larger than the largest transmission band in the Poincaré surface of section. "Noiseless scattering states" appear in $H(x,p)$ in form of pronounced density enhancements at the position of the largest transmission bands and a strongly reduced amplitude elsewhere. In the bottom two bars the shutter openings ($w/d = 0.2$) are reduced, giving rise to a classical phase space structure in which all transmission bands are smaller than the Planck cell h. For this configuration the Husimi distribution $H(x,p)$ practically covers the whole phase space, with only small enhancements near the largest transmission bands.

realized in the ballistic and the stochastic limit: In the ballistic case, noiseless states should appear in $P(T)$ in the form of eigenvalues that accumulate right at the classical values $T = 0$ and $T = 1$. Due to stochastic scattering, such accumulations should be suppressed in the presence of disorder.

We now search for signatures of these differences in the numerical results for $P(T)$ as we record them along the crossover trajectories (1) and (2). In order to better resolve the behavior of $P(T)$ near the crucial value $T = 1$ we plot the integrated eigenvalue distribution[10, 11, 15] $I(T) = \int_T^1 P(\tau)d\tau$. At those cavity parameters $V_0 = 0$ and $w = d/2$ from which both trajectories (1) and (2) start out, conditions are very favorable to the appearance of noiseless scattering channels. Accordingly, we indeed find that $I(T)$ features a very pronounced offset at $T \approx 1$ (see Fig. 3a), corresponding to a statistically significant portion of effectively noiseless eigenvalues $T > 0.999$. These *classical* transmission eigenvalues should be due to *direct scattering processes* which connect the entrance with the exit in such a way that the cavity dwell time τ_D is minimized. In crossover (1) the weight of these direct processes is now gradually reduced by a decrease of the the cavity openings w. We should therefore find that also the offset in $I(T)$ is gradually reduced in this crossover. Our numerical results (Fig. 3a) indeed confirm this reasoning, demonstrating how the distribution $I(T)$ shifts towards its RMT-limt [Eq. (4)] for $w \to 0$. This behavior is all the more interesting as our sharp cavity openings do give rise to diffractive scattering[12, 20, 21] which
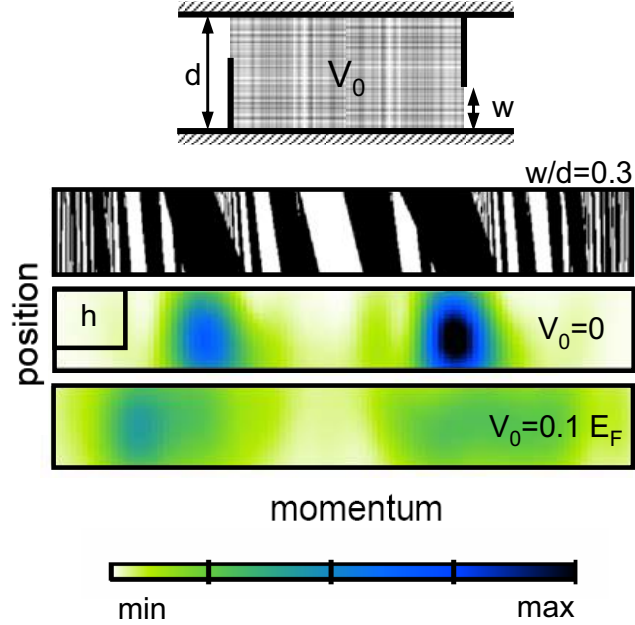
Figure 5. Classical phase space and Husimi distribution $H(x,p)$ for the cavity of Fig. 1a at fixed opening ratio $w/d = 0.3$ (same color coding as in Fig. 4). Top two bars: No disorder. Bottom bar: Moderate disorder, $V_0 = 0.1E_F$. Bulk disorder destroys the appearance of noiseless states due to stochastic scattering.

might suppress the formation of noiseless states. Our observation suggests, however, that noiseless transmission can still occur when scattering states effectively bypass any diffractive corners.[11, 15] In tcrossover (2) the evolution of $I(T)$ should be different: Starting from the same initial values $V_0 = 0$ and $w = d/2$ as for crossover (1), we now gradually increase the bulk disorder strength up to values of $V_0 = 0.1 \times E_F$. Bulk disorder cannot be bypassed by any transmitting state and should therefore destroy the noiseless channels and, consequently, the offset in $I(T)$. We find that already a small disorder potential ($V_0 = 0.03 \times E_F$) suppresses the offset in $I(T)$ entirely (Fig. 3b). With higher values of V_0 we reach the RMT-limit for $I(T)$. The striking difference between the ballistic crossover (1) in Fig. 3a and the stochastic crossover (2) in Fig. 3b is best visualized by zooming into the distribution $I(T)$ at values close to $T = 1$ where the gradual vs. "sudden" suppression of the offset becomes most apparent (see insets in Figs. 3a,b). The observation that $I(T)$ depends on the specific character of the diffractive scattering ("bulk vs. surface disorder") is in line with recent investigations.[10–12, 14, 15] To the best of our knowledge, the present results explicitly demonstrate for the first time in a genuine 2D system, how these different noise sources influence the emergence of noiseless scattering states.

The above results should also be reflected in the degree with which the quantum scattering process can resolve the underlying classical phase space. To investigate this issue explicitly, we compare Husimi distributions of scattering states with the Poincaré surface of section recorded at the entrance lead mouth.[9] We calculate the cumulative Husimi function containing those eigenstates $|T_i\rangle$ of $t^\dagger t$ which correspond to the largest transmission eigenvalues T_i within a given energy interval,

$$H(x,p) = \sum_i^M H_i(x,p) = \sum_i^M |\langle T_i | x, p \rangle|^2 . \tag{7}$$

$|x,p\rangle$ is a coherent state of minimum uncertainty with its peak at the position x, p and the number of eigenstates $|T_i\rangle$ that contribute to the above sum is chosen as $M = 2N$. In line with our calculations for the integrated eigenvalue distribution $I(T)$ (see Fig. 3), we now probe how the cavity opening and disorder strength affect the distribution $H(x,p)$. In our calculations we keep the electron energy fixed in the averaging interval $k_F \in [40.1, 40.85] \times \pi/d$ and vary the cavity opening w [as in crossover (1)] or, alternatively, the disorder strength V_0 [as in crossover (2)].

In the ballistic crossover (1) we can obtain a good measure for the onset thresholds of the "noiseless" states by comparing the size of the Planck cell h (indicated by the black frames in Fig. 3) to the area A^{band} of the largest transmission band (see large black regions in the classical Poincaré surface). By tuning the cavity openings at fixed energy E_F we change the size of A^{band} at a fixed value of h. When these two phase space areas are equal in size, $A^{\mathrm{band}} = h$, we can therefore obtain a threshold value for the appearance of the first noiseless state in terms of the cavity opening: $w/d \approx 0.32$. Comparing this estimate with our numerical results for $H(x,p)$ (see Fig. 4) yields very good agreement: Whereas for an opening of $w/d = 0.2 < 0.32$ the Husimi function $H(x,p)$ looks rather flat (Fig. 4 bottom), for $w/d = 0.4 > 0.32$ (Fig. 4 top) the function $H(x,p)$ displays very clear enhancements around the largest transmission bands and a strongly reduced amplitude elsewhere. Since the largest transmission bands correspond to the classical "direct scattering processes", our results confirm that the noiseless states are indeed caused by direct processes with very short dwell times τ_D.

Whereas the degree of quantum-to-classical corrspondence is remarkably good in the ballistic limit, the presence of disorder [as in crossover (2)] destroys this correspondence. In Fig. 5 we demonstrate this behavior by comparing the Husimi distribution for a ballistic and a disordered cavity, respectively. We find that, as expected, the bulk disorder in the cavity destroys any noiseless states by strongly reducing any pronounced enhancements which would otherwise be present in $H(x,p)$. The suppression of the noiseless states, in turn, impairs the degree of quantum-to-classical correspondence of the scattering process.

5. OUTLOOK

In our eyes it would be interesting to study how the above crossovers are reflected in transport quantities like the weak localization correction to the conductance or the parametric conductance fluctuations. For both these quantities it was recently investigated how the emergence of noiseless scattering states modifies the previously established predictions from random matrix theory.[10, 18] The numerical model presented in this manuscript should allow to test these predictions as well as the influence of disorder in detail. Note that such investigations could also be extended to ballistic cavities with regular vs. chaotic classical dynamics, in line with recent shot noise studies on such systems.[12–14, 23–25]

6. SUMMARY

To summarize, we have numerically determined the behavior of the Fano factor F in a realistic scattering system with a tunable disorder potential and tunable shutters. We find that diffraction at the lead openings is sufficient to establish the RMT prediction for shot noise suppression ($F = 1/4$), irrespective of disorder in the cavity. The disordered-to-ballistic crossover in F can be estimated by a generalization of a previously proposed dependence[8] on the quantum scattering time τ_Q [Eq. (3)], provided that the definition of τ_Q is properly modified to include diffraction at the cavity openings. We find specific signatures of ballistic vs. stochastic scattering in the distribution of transmission eigenvalues T near the classical values $T = 0, 1$. We thereby provide the first evidence for "noiseless scattering states"[8] in genuine 2D-cavities and confirm predictions on the decomposition of the electronic flow in a classical and a quantum component.[10] The numerically determined onset thresholds for the "classical" states are in very good agreement with analytical estimates based on a classical phase space analysis. As anticipated, noiseless scattering states disappear in the presence of bulk disorder which acts as a source of stochastic scattering.[11]

REFERENCES

1. W. Schottky, Ann. Phys. (Leipzig) **57**, 541 (1918).
2. C. W. J. Beenakker and Ch. Schönenberger, Physics Today **56(5)**, 37 (2003).
3. Ya. M. Blanter and M. Büttiker, Phys. Rep. **336**, 1 (2000).
4. S. Oberholzer, E. V. Sukhorukov and Ch. Schönenberger, Nature **415**, 765 (2002).
5. X. Jehl, M. Sanquer, R. Calemczuk, and D. Mailly, Nature **405**, 50 (2000).
6. C. W. J. Beenakker and H. van Houten, Phys. Rev. B **43**, R12066 (1991).
7. O. Agam, I. Aleiner, and A. Larkin, Phys. Rev. Lett. **85**, 3153 (2000).
8. P. G. Silvestrov, M. C. Goorden, and C. W. J. Beenakker, Phys. Rev. B **67**, 241301(R) (2003).
9. J. Tworzydło, A. Tajic, H. Schomerus, and C. W. J. Beenakker, Phys. Rev. B **68**, 115313 (2003).
10. Ph. Jacquod and E. V. Sukhorukov, Phys. Rev. Lett. **92**, 116801 (2004).
11. E. V. Sukhorukov and O. M. Bulashenko, Phys. Rev. Lett. **94**, 116803 (2005).
12. F. Aigner, S. Rotter, and J. Burgdörfer, Phys. Rev. Lett. **94**, 216801 (2005).
13. P. Marconcini, M. Macucci, G. Iannaccone, B. Pellegrini, and G. Marola, Europhys. Lett. **73**, 574 (2006).
14. S. Rotter, F. Aigner, and J. Burgdörfer, Phys. Rev. B **75**, 125312 (2007).
15. Ph. Jacquod and R. S. Whitney, Phys. Rev. B **73**, 195115 (2006); Proceedings of the Fourth International Conference on Unsolved Problems of Noise and Fluctuations in Physics, Biology, and High Technology, AIP Conf. Proc. **800**, 225 (2005).
16. H. U. Baranger and P. A. Mello, Phys. Rev. Lett. **73**, 142 (1994); R. A. Jalabert, J.-L. Pichard, and C. W. J. Beenakker, Europhys. Lett. **27**, 255 (1994).
17. M. A. Topinka, B. J. LeRoy, R. M. Westervelt, S. E. J. Shaw, R. Fleischmann, E. J. Heller, K. D. Maranowski, A. C. Gossard, Nature **410**, 283 (2001).
18. S. Rahav and P. W. Brouwer, Phys. Rev. Lett. **95**, 056806 (2005).
19. S. Rotter, J.-Z. Tang, L. Wirtz, J. Trost, and J. Burgdörfer, Phys. Rev. B **62**, 1950 (2000); S. Rotter, B. Weingartner, N. Rohringer, and J. Burgdörfer, Phys. Rev. B **68**, 165302 (2003).
20. L. Wirtz, J.-Z. Tang, and J. Burgdörfer, Phys. Rev. B **56**, 7589 (1997); **59**, 2956 (1999).
21. L. Wirtz, C. Stampfer, S. Rotter, and J. Burgdörfer, Phys. Rev. E **67**, 016206 (2003).
22. J. Burgdörfer and J. Gibbons, Phys. Rev. A, **42**, 1206 (1990).
23. H.-S. Sim and H. Schomerus, Phys. Rev. Lett. **89**, 066801 (2002).
24. R. G. Nazmitdinov, H.-S. Sim, H. Schomerus, and I. Rotter, Phys. Rev. B **66**, 241302(R) (2002).
25. V. A. Gopar, S. Rotter, and H. Schomerus, Phys. Rev. B **73**, 165308 (2006).